RSC Advances

ROYAL SOCIETY OF CHEMISTRY

www.rsc.org/advances

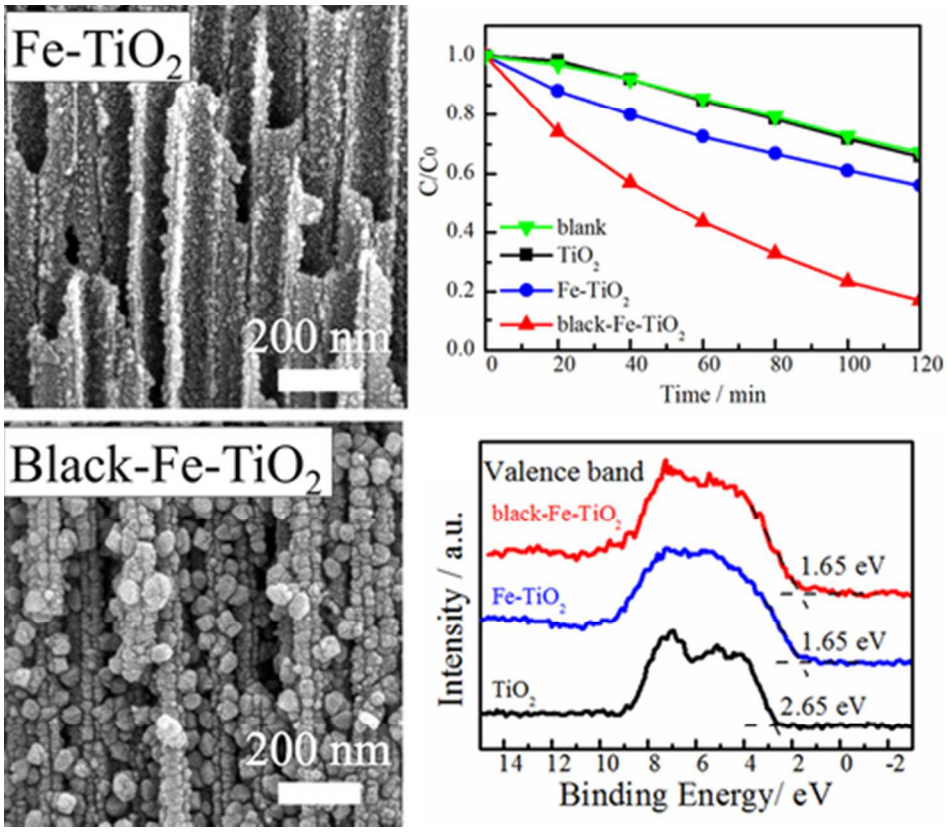

Graphical Abstract
39x34mm (300 x 300 DPI)

RSC Advances

RSCPublishing

COMMUNICATION

Visible light induced photocatalytic activity of Fe^{3+}/Ti^{3+} co-doped TiO_2 nanostructures

Cite this: DOI: 10.1039/x0xx00000x

Bo Chen, [a] * Andrew J. Haring, [b] Jeremy A. Beach, [b] Menghui Li, [c] Grayson S. Doucette, [c] Amanda J. Morris, [b] Robert B. Moore, [b] Shashank Priya [a] *

Received 00th January 2012,
Accepted 00th January 2012

DOI: 10.1039/x0xx00000x

www.rsc.org/

Black TiO_2 nanostructures co-doped with Fe^{3+} and Ti^{3+} were synthesized by annealing Fe-deposited TiO_2 nanotubes in vacuum. These vacuum-annealed samples exhibited improved visible light absorption and efficient photocatalytic activity under visible light illumination as compared to conventional TiO_2 materials. XPS and EPR spectra confirmed the presence of Ti^{3+} in the bulk and Fe^{3+} dopant.

Since discovery of photoelectrochemical water splitting using a TiO_2 photoanode by Fujishima and Honda,[1] TiO_2-based photocatalysis has attracted much attention due to its promising photocatalytic performance, chemical stability, photocorrosion resistance, and low cost.[2, 3] However, TiO_2 exhibits a large band gap (3.2 eV for anatase and brookite, 3.0 eV for rutile) and can only be activated by UV light irradiation, which occupies only a small fraction of the total incident sunlight (3-5%).[4-6] Therefore, significant efforts have to be made to extend the working spectrum of TiO_2 photocatalysis activity into the visible light region, which accounts for 43% of the total incident sunlight. Doping of various transition metals (Fe, Nb, Co, Ni, and V) and nonmetal ions (such as C, N, and S) are the most common strategies utilized to reduce the band gap of TiO_2.[7-10] Due to its environmental friendliness and natural abundance, Fe distinguishes itself from the various choices for dopants and has shown good conversion efficiency in the visible light region.[11-16] Recently, reduced TiO_2 with self-doped Ti^{3+} has been shown as an effective strategy to extend the photoresponse from UV to visible light regions.[17-21] Black hydrogenated TiO_2 nanoparticles with 1.0 eV band gap were prepared in a high-pressure H_2 atmosphere.[17] Ti^{3+}-doped TiO_2, produced by reducing titanium precursors with CO and NO, exhibited high visible light water splitting activity.[18] Additionally, reduced TiO_2 synthesized by hydrothermal treatment of TiH_2 in H_2O_2 aqueous solution demonstrated enhanced visible-light-induced photocatalytic behaviour.[19] The effect of co-doping of Fe^{3+} and Ti^{3+} on TiO_2 for photocatalytic application has been seldom studied. Here we report the fabrication of novel material, Fe^{3+}/Ti^{3+} co-doped TiO_2 nanostructures, by annealing the TiO_2 nanotubes with electrodeposited $Fe(OH)_3$ nanoparticles under vacuum conditions. Using this material, the synergistic effects between Ti^{3+} and Fe^{3+} dopants on photocatalytic performance were investigated.

Highly ordered TiO_2 nanotube arrays were synthesized by typical two-step anodization in an ethylene glycol electrolyte containing 0.3 wt% NH_4F and 2 vol% DI water. The TiO_2 nanotubes grew to a length of 12 μm under 60 V applied potential for 30 min. Iron hydroxide were electrochemically deposited onto the as-anodized TiO_2 nanotubes using potential cycling in a 5 mM $FeCl_3$ aqueous solution containing 5 mM KF, 0.1 M KCl, and 1M H_2O_2 at a scan rate of 20 mV/s from -0.4 to 0.5 V *vs* Ag/AgCl for 50 cycles. Subsequently, the Fe-deposited samples were sealed in quartz tube under a 10^{-6} Torr vacuum and annealed at 450 ºC for 2 h with a heating and cooling rate of 2 ºC/min. In comparison, some as-anodized and Fe-deposited TiO_2 nanotubular samples were annealed in air at 450 ºC for 2 h.

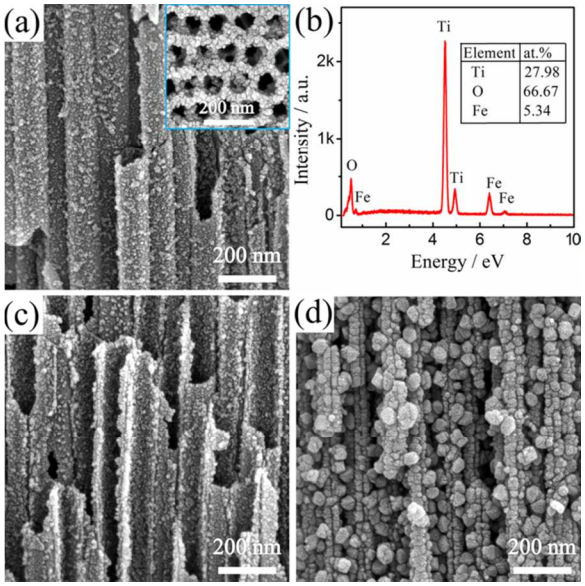

Fig. 1. (a) SEM image of Fe-deposited TiO_2 nanotubes and the inset is corresponding top surface; (b) EDS spectrum of Fe-deposited TiO_2 nanotubes; SEM image of Fe-deposited TiO_2 nanotubes after sintering in (c) air atmosphere and (d) vacuum condition.

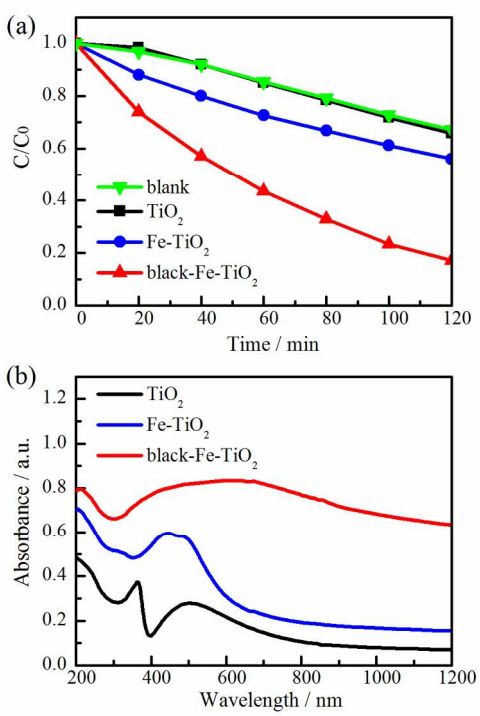

Fig. 2. (a) Visible light photocatalytic activities and (b) UV-vis-NIR absorbance of nanotubular TiO_2, Fe-TiO_2, and black-Fe-TiO_2 samples.

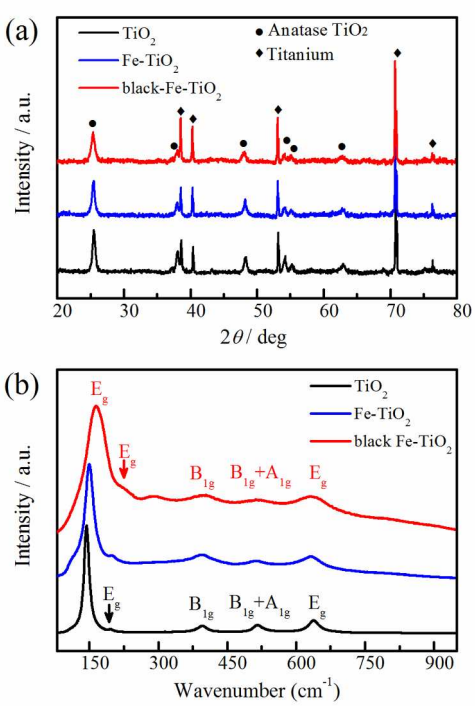

Fig. 3 (a) XRD patterns and (b) Raman spectra for nanotubular TiO_2, Fe-TiO_2, and black-Fe-TiO_2 samples.

After electrodeposition for 50 potential cycles, the Fe-deposited sample exhibited a gold colour, and $Fe(OH)_3$ nanoparticles were successfully precipitated on both the top surface and the inner surface of TiO_2 nanotubes (Fig. 1a). The corresponding EDS spectrum in Fig. 1b indicates the atomic percentage of Fe was 5.34 %. During electrodeposition, reduction of hydrogen peroxide created OH^- groups on the nanotube surface, which promoted the formation of $Fe(OH)_3$ precipitates.[22] The KF solution was added to facilitate the formation of FeF^{2+} complex that avoided the reduction of Fe^{3+} ions to Fe^{2+} ions during electrodeposition. This ensured that the hydrogen peroxide could be reduced and reacted with FeF^{2+} to form $Fe(OH)_3$ precipitates.

After annealing the Fe-deposited TiO_2 nanotubes in air at 450 ºC for 2 h, the colour changed to brown, referred to as Fe-TiO_2. On the other hand, when annealing the Fe-deposited samples in 10^{-6} Torr vacuum at 450 ºC for 2 h, the colour changed to black, referred to as black-Fe-TiO_2. As shown in Fig. 1c and d, both Fe-TiO_2 and black-Fe-TiO_2 samples maintained nanotubular morphologies, while the decorated nanoparticles significantly enlarged to 30-100 nm after vacuum annealing.

The photocatalytic activities of nanotubular TiO_2, Fe-TiO_2, and black-Fe-TiO_2 samples were evaluated by methylene blue (MB) degradation under visible light illumination (Fig. 2a). Visible light was created by applying an ultraviolet cut-off filter (cut-off wavelength at 400 nm) to the solar simulator. Compared to blank experiments without any catalyst, air-sintered nanotubular TiO_2 samples showed negligible degradation of MB solution. Enhanced photocatalytic activity under visible light was observed for the Fe-TiO_2 samples. The black-Fe-TiO_2 samples exhibited significantly improved degradation rate of MB solution. The UV-Vis-NIR absorption spectra shown in Fig. 2b was used to identify that the light absorption for different TiO_2 samples. The black-Fe-TiO_2 samples displayed an enhanced broad absorption peak around 330-900 nm, which was ascribed to the co-doping of Fe^{3+} and Ti^{3+}, as discussed later. Fe-TiO_2 nanotubes revealed a pronounced peak at 360-600 nm, explaining the visible light photocatalytic activity and linking the efficiency to the Fe ions. The air-sintered TiO_2 nanotubes absorb mainly the UV light with an additional weak peak present around 400-650 nm. This weak peak is consistent with the previous reports but its origin is still being debated, which maybe come from N^- and F^- impurites produced during the anodization.[15, 23, 24]

The structural properties for Fe-TiO_2 and black-Fe-TiO_2 samples were characterized by XRD patterns and Raman spectra. XRD patterns for air-sintered TiO_2, Fe-TiO_2, and black-Fe-TiO_2 samples all exhibited only the crystalline anatase phase (Fig. 3a). No Fe, FeO, or Fe_2O_3 related phase could be observed in XRD patterns, thus all Fe ions were incorporated into the TiO_2 lattice as dopants. Raman spectra were acquired using a Raman spectrometer with a laser excitation of 532 nm. Raman spectra of all samples displayed six ($3E_g + 2B_{1g} + A_{1g}$) Raman-active modes (Fig. 3b), which indicated that anatase TiO_2 is the predominant phase. Furthermore, no peaks ascribed to iron oxide appeared, which is consistent with the XRD results. Due to the doping of Fe ions in Fe-TiO_2 samples, the centre position for most intense E_g peak was blue-shifted from 143.8 cm^{-1} to 149.7 cm^{-1} and the corresponding width was broadened from 13.1 cm^{-1} to 21.6 cm^{-1}. Black-Fe-TiO_2 samples displayed further blue-shifting and broadening of the E_g peak. Moreover, a new Raman peak appeared at 292 cm^{-1} for black-Fe-TiO_2 samples. This peak illustrates the structural changes that occurred for black-Fe-TiO_2 samples due to annealing in an oxygen poor environment, which broke down the Raman selection rule and activated the Raman forbidden mode.

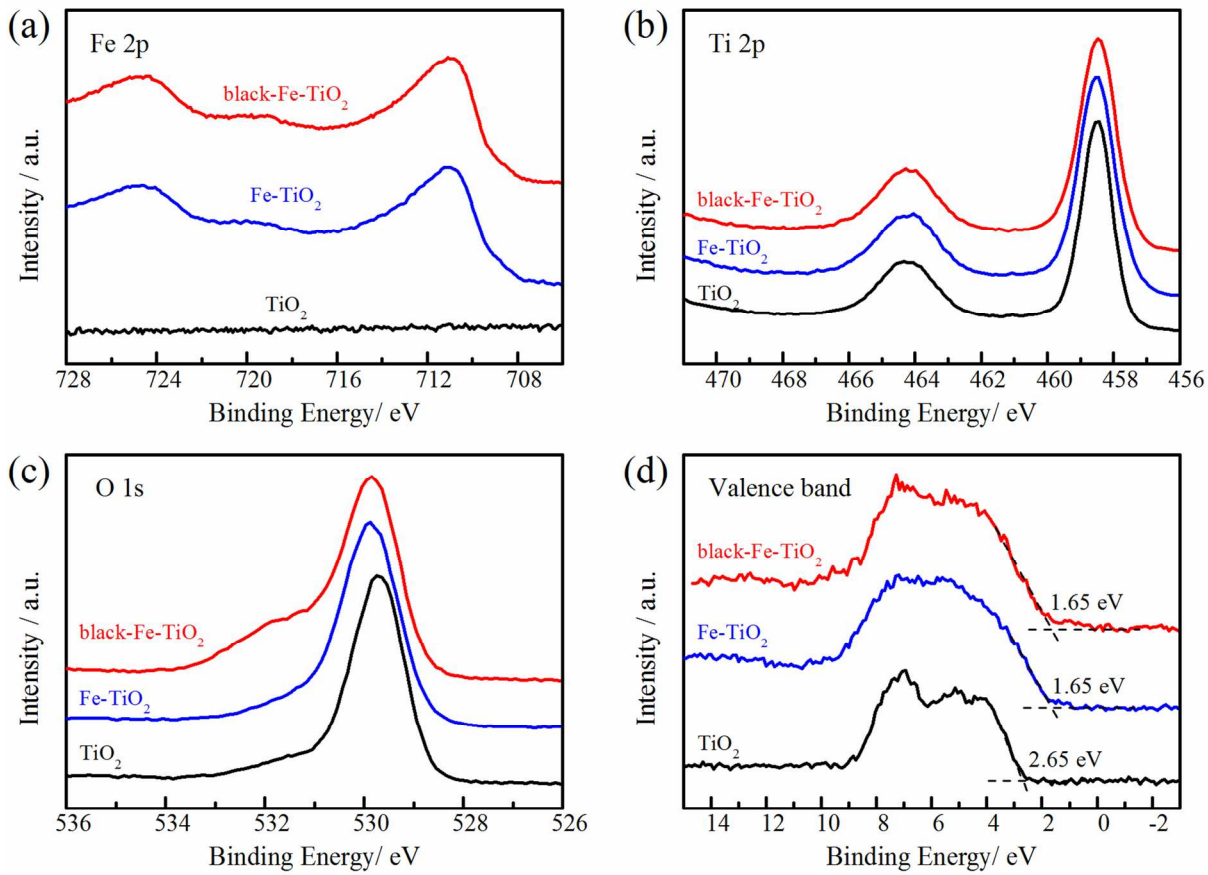

Fig. 4 (a) Fe 2p, (b) Ti 2p, (c) O 1s, and (d) valence band XPS spectra of nanotubular TiO_2, Fe-TiO_2, and black-Fe-TiO_2 samples.

The electronic properties of Fe-TiO_2 and black-Fe-TiO_2 nanostructures were explored by X-ray photoelectron spectroscopy (XPS) and electron paramagnetic resonance (EPR). XPS spectra can explore the surface chemical bonding of Fe-TiO_2 and black-Fe-TiO_2 nanostructures. XPS spectra were recorded by a scanning photoelectron spectrometer microprobe using Al Kα radiation at a power of 50 W with pass energy of 26 eV. The bind energy was calibrated by referencing the C 1s peak at 284.6 eV. As shown in Fig. 4a, the dominant Fe 2p XPS peaks for both Fe-TiO_2 and black-Fe-TiO_2 samples located at 724.6 and 711.0 eV, are consistent with the binding energies of Fe^{3+} $2p_{1/2}$ and $2p_{3/2}$, respectively.[15, 16] This revealed that Fe^{3+} was the predominant charge state of Fe dopant. Compared with air-sintered TiO_2 nanotubes, Ti 2p XPS spectra of Fe-TiO_2 and black-Fe-TiO_2 samples showed no significant differences (Fig. 4b), which indicated there is no Ti^{3+} present at the surface. However, the XPS cannot detect whether there is any Ti^{3+} in the bulk or not, thus we further utilized the ERP spectra to examine the Ti^{3+} in bulk.

EPR spectra were collected at room temperature by Bruker ER 200D-SRC electron spin resonance. EPR provides detailed information for both the nature of species and their coordination symmetries in the solid. As shown in Fig. 5, there was no presence of EPR features for air-sintered TiO_2 nanotubes. Typically, the Fe^{3+} species show a broad "step" EPR signal around g = 1.935 because Fe^{3+} substituted for Ti^{4+} in the TiO_2 lattice.[25, 26] The EPR spectra of Fe-TiO_2 and black-Fe-TiO_2 samples both reveal a broad "step" signal around g = 1.935, which demonstrate the doping of Fe^{3+}. Based on the literature, we know the Ti^{3+} in the bulk TiO_2 will exhibit an intense EPR signal.[21] In Fig. 5 we examined the EPR spectra of vacuum-sintered TiO_2 sample (TiO_2-vacuum) and black-Fe-TiO_2 sample, both of them demonstrated a very narrow EPR signal at g= 1.937, which indicated the presence of Ti^{3+} in the bulk TiO_2. These Ti^{3+} species were created due to the reduction of Ti^{4+} by vacuum annealing. In a word, the black-Fe-TiO_2 samples, it not only showed the broad "step" EPR signal related to Fe^{3+} doping, but also exhibited an intense narrow EPR peak due to the present of Ti^{3+}. These results confirmed the co-doping of Fe^{3+} and Ti^{3+} in black-Fe-TiO_2 samples.

Due to the surface Ti-OH groups and lattice Ti-O groups, the O 1s region of Fe-TiO_2 and black-Fe-TiO_2 samples can be deconvoluted into two peaks centered at 531.7 and 529.8 eV, respectively (Fig. 4c). The lattice Ti-O groups of Fe-TiO_2 and black-Fe-TiO_2 samples shifted binding energy positively by 0.15 eV compared with the TiO_2 nanotubes. This shift was motivated by the Ti-O-Fe bonds and the interaction between Fe^{3+} and Ti^{4+}. Furthermore, the black-Fe-TiO_2 samples displayed more surface Ti-OH bonds than Fe-TiO_2 samples. The valence band edge of vacuum-sintered TiO_2 was as same as the air-sintered TiO_2 nanotubes, while the valence band edge of both Fe-TiO_2 and black-Fe-TiO_2 samples blue-shifted by 1.0 eV (Fig. 4d).

The above analysis enables us to understand the mechanism for the enhanced visible light photocatalytic performance for Fe-TiO_2 and black-Fe-TiO_2 nanostructures. The crystalline anatase phase and one-dimensional nanotubular structures avoid any significant charge recombination and facilitate the rapid electron-hole separation. Doping the TiO_2 nanotubes with Fe^{3+} blue-shifts the valence band

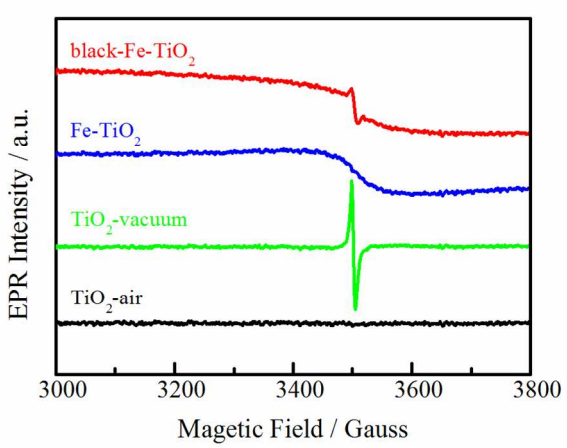

Fig. 5 EPR spectra for air-sintered-TiO_2, vacuum-sintered-TiO_2, Fe-TiO_2, and black-Fe-TiO_2 samples.

edge and induces a remarkable narrowing of bandgap, thereby enabling the visible light photocatalytic activity. Annealing in vacuum conditions reduces the Fe-doped TiO_2 nanotubes and produces Fe^{3+}/Ti^{3+} co-doped black-Fe-TiO_2 samples. Aside from the modification of valence band edge caused by Fe^{3+} dopant, the Ti^{3+} species in the bulk introduces localized states at 0.75-1.18 eV below the conduction band minimum of TiO_2.[20] Therefore, synergistic effects between Ti^{3+} and Fe^{3+} species in black-Fe-TiO_2 samples further narrow the bandgap and promote enhanced photocatalytic performance in the visible light range.

Conclusions

In summary, TiO_2 nanostructures with Fe^{3+} doping and Fe^{3+}/Ti^{3+} co-doping were synthesized through annealing Fe-deposited TiO_2 nanotubes in air atmosphere and vacuum, respectively. The Fe-doped TiO_2 samples showed visible light induced photocatalytic activity; the Fe^{3+}/Ti^{3+} co-doped TiO_2 samples displayed a black colour and further enhanced photocatalytic performance under visible light illumination. Fe^{3+} doping blue-shifted the valence band edge of TiO_2 by 1.0 eV, which allowed visible light absorption. Annealing in vacuum produced self-doped Ti^{3+} in the bulk, and the synergistic effects between Ti^{3+} and Fe^{3+} dopants in black-Fe-TiO_2 samples significantly narrowed the band gap, leading to efficient photocatalytic performance in the visible light range.

Acknowledgement

The authors gratefully acknowledge the financial support from National Science Foundation through Fundamental Research Program.

Notes and references

[a] Center for Energy Harvesting Materials and Systems, Virginia Tech, 24061 USA. Fax: (540) 231-0745; Tel: (540) 808-3623; E-mail: bochen09@vt.edu, spriya@vt.edu
[b] Department of Chemistry, Virginia Tech, Blacksburg, VA 24061 USA
[c] Department of Materials Science and Engineering, Virginia Tech, Blacksburg, VA 24061 USA

1. A. Fujishima and M. Honda, *Nature*, 1972, **238**, 37-38.
2. M. Gratzel, *Nature*, 2001, **414**, 338-344.
3. X. B. Chen, S. H. Shen, L. J. Guo and S. S. Mao, *Chem. Rev.*, 2010, **110**, 6503-6570.
4. S. U. M. Khan, M. Al-Shahry and W. B. Ingler, *Science*, 2002, **297**, 2243-2245.
5. I. S. Cho, C. H. Lee, Y. Z. Feng, M. Logar, P. M. Rao, L. L. Cai, D. R. Kim, R. Sinclair and X. L. Zheng, *Nat. Commun.*, 2013, **4**, 1723.
6. J. Shi and X. D. Wang, *Energy Environ. Sci.*, 2012, **5**, 7918-7922.
7. I. Paramasivam, H. Jha, N. Liu and P. Schmuki, *Small*, 2012, **8**, 3073-3103.
8. S. G. Kumar and L. G. Devi, *J. Phys. Chem. A*, 2011, **115**, 13211-13241.
9. Y. C. Nah, I. Paramasivam and P. Schmuki, *Chemphyschem*, 2010, **11**, 2698-2713.
10. J. Choi, H. Park and M. R. Hoffmann, *J. Phys. Chem. C*, 2010, **114**, 783-792.
11. Q. L. Jin, M. Fujishima and H. Tada, *J. Phys. Chem. C*, 2011, **115**, 6478-6483.
12. H. Tada, Q. Jin, H. Nishijima, H. Yamamoto, M. Fujishima, S. Okuoka, T. Hattori, Y. Sumida and H. Kobayashi, *Angew. Chem. Int. Ed.*, 2011, **50**, 3501-3505.
13. M. Liu, X. Q. Qiu, M. Miyauchi and K. Hashimoto, *J. Am. Chem. Soc.*, 2013, **135**, 10064-10072.
14. R. Su, R. Bechstein, J. Kibsgaard, R. T. Vang and F. Besenbacher, *J. Mater. Chem.*, 2012, **22**, 23755-23758.
15. Z. H. Xu and J. G. Yu, *Nanoscale*, 2011, **3**, 3138-3144.
16. Q. P. Wu, Q. Zheng and R. van de Krol, *J. Phys. Chem. C*, 2012, **116**, 7219-7226.
17. X. B. Chen, L. Liu, P. Y. Yu and S. S. Mao, *Science*, 2011, **331**, 746-750.
18. F. Zuo, L. Wang, T. Wu, Z. Zhang, D. Borchardt and P. Feng, *J. Am. Chem. Soc.*, 2010, **132**, 11856-11857.
19. X. Liu, S. Gao, H. Xu, Z. Lou, W. Wang, B. Huang and Y. Dai, *Nanoscale*, 2013, **5**, 1870-1875.
20. G. Wang, H. Wang, Y. Ling, Y. Tang, X. Yang, R. C. Fitzmorris, C. Wang, J. Z. Zhang and Y. Li, *Nano Lett.*, 2011, **11**, 3026-3033.
21. A. Naldoni, M. Allieta, S. Santangelo, M. Marelli, F. Fabbri, S. Cappelli, C. L. Bianchi, R. Psaro and V. Dal Santo, *J. Am. Chem. Soc.*, 2012, **134**, 7600-7603.
22. R. Schrebler, K. Bello, F. Vera, P. Cury, E. Munoz, R. del Rio, H. G. Meier, R. Cordova and E. A. Dalchiele, *Electrochem. Solid-State Lett.*, 2006, **9**, C110-C113.
23. Z. H. Zhang and P. Wang, *Energy Environ. Sci.*, 2012, **5**, 6506-6512.
24. Z. W. Liu, W. B. Hou, P. Pavaskar, M. Aykol and S. B. Cronin, *Nano Letters*, 2011, **11**, 1111-1116.
25. Y. Cong, J. L. Zhang, F. Chen, M. Anpo and D. N. He, *J. Phys. Chem. C*, 2007, **111**, 10618-10623.
26. K. Nagaveni, M. S. Hegde and G. Madras, *J. Phys. Chem. B*, 2004, **108**, 20204-20212.

